



Article

<https://doi.org/10.1038/s44220-025-00501-8>

Regional adiposity shapes brain and cognition in adults

Received: 19 March 2025

Accepted: 19 August 2025

Published online: 15 September 2025

Check for updates

Die Zhang^{1,9}, Yingji Fu^{1,9}, Chenye Shen^{1,9}, Chaoqiang Liu², Nanguang Chen^{1,2,3}, Hua Cao⁴, Kui Kai Lau^{5,6} & Anqi Qiu^{1,2,7,8}

Body mass index (BMI) is commonly used to assess obesity, but it fails to capture the complexities of regional adiposity, which can have varying effects on brain health. This study analyzed data from over 18,000 UK Biobank participants to investigate the relationship between regional adiposity, measured using dual-energy X-ray absorptiometry, and brain health, evaluated through multimodal brain imaging and cognitive tests. Adiposity in the arm, leg, trunk and visceral regions was differentially associated with brain morphology, functional connectivity and white-matter integrity in the sensorimotor, limbic, default mode and subcortical–cerebellar–brainstem systems. The aging of these four brain systems was indexed by brain age gap (BAG), with cortical-related BAGs (sensorimotor, limbic, default mode) mediating relationships between visceral adiposity and cognitive performance in reasoning, executive function, processing speed and memory. These results highlight the importance of considering regional adiposity, beyond BMI, in characterizing its associations with brain and cognitive aging.

Obesity has emerged as a global health challenge with far-reaching implications for physical and cognitive well-being^{1,2}. Although body mass index (BMI) is traditionally used as a proxy of general obesity, it cannot accurately capture regional variations in adiposity across the body. Emerging evidence is highlighting that fat accumulation in different body regions poses distinct risks for clinical outcomes, including Alzheimer's disease and cognitive decline³, emphasizing the importance of moving beyond BMI as a sole indicator of obesity. This is particularly critical in middle-aged and older adults, who are at increased risk of cognitive decline and neurodegeneration associated with obesity^{4,5}.

A growing body of research is highlighting the negative impact of obesity, as measured by BMI, waist circumference and waist-to-hip ratio, on brain health and cognitive function^{6–9}. Obesity has been associated with structural and functional brain changes, including reduced

gray-matter volume, disrupted white-matter integrity and dysregulated functional connectivity^{7–9}. These changes may reflect accelerated brain aging. Moreover, obesity has consistently been associated with declines in multiple cognitive domains, such as working memory and executive function, which are key indicators of cognitive aging^{10,11}. Overall, these findings highlight the complex interplay of obesity, brain aging and cognitive decline, suggesting that targeting obesity could be crucial for preserving brain health and mitigating age-related cognitive deterioration.

However, existing research on the relationship between obesity and brain aging has largely relied on BMI, overlooking the potential differential effects of regional adiposity. Adipose tissue plays diverse biological roles that may have critical implications for brain health. For example, visceral adipose tissue (VAT) is strongly associated with metabolic syndromes and cardiovascular disease, and its secretion

¹Department of Health Technology and Informatics, The Hong Kong Polytechnic University, Hung Hom, Hong Kong. ²Department of Biomedical Engineering, National University of Singapore, Singapore, Singapore. ³NUS (Suzhou) Research Institute, Suzhou, China. ⁴Fuzhou University Affiliated Provincial Hospital, Fujian, China. ⁵School of Clinical Medicine, LKS Faculty of Medicine, The University of Hong Kong, Hong Kong, Hong Kong. ⁶State Key Laboratory of Brain and Cognitive Sciences, The University of Hong Kong, Hong Kong, Hong Kong. ⁷Mental Health Research Centre, The Hong Kong Polytechnic University, Hung Hom, Hong Kong. ⁸Department of Biomedical Engineering, Johns Hopkins University, Baltimore, MD, USA. ⁹These authors contributed equally: Die Zhang, Yingji Fu. e-mail: an-qi.qiu@polyu.edu.hk

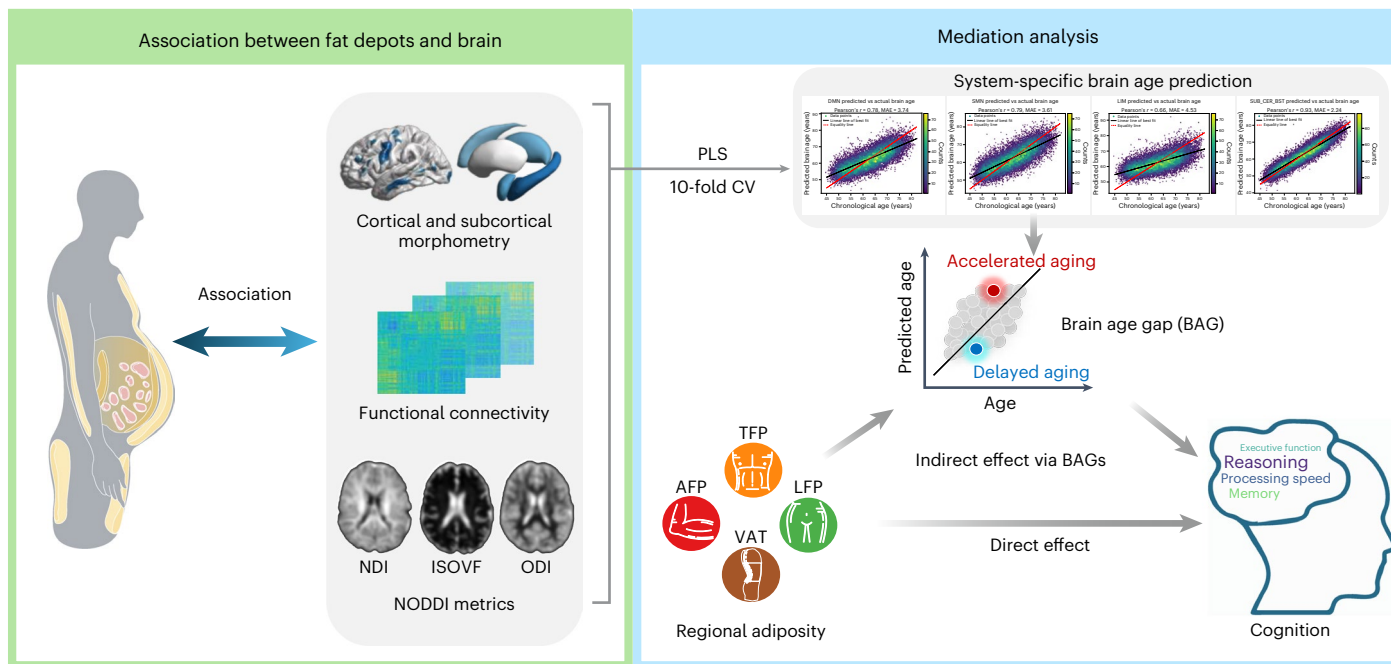


Fig. 1 | Schematic overview of the study design. The left panel illustrates the associations between regional adiposity and brain morphology, functional connectivity and white-matter microstructure. The right panel depicts the construction of a brain age prediction model using multimodal imaging

parameters, with the resulting BAGs serving as mediators in the subsequent analysis of the relationship between regional adiposity and cognitive function. CV, cross-validation; PLS, partial least squares; MAE, mean absolute error.

of pro-inflammatory cytokines (for example, tumor necrosis factor-alpha (TNF- α) and interleukin-6) has been linked to blood–brain barrier disruption, neuroinflammation and neurodegeneration^{12,13}. Limb fat accumulation, often accompanied by muscle mass loss, may impact brain health through mechanisms such as impaired mitochondrial function, reduced energy metabolism and increased oxidative stress^{14–16}. In contrast, certain fat deposits, such as lower-body fat, may have protective effects by improving insulin sensitivity and reducing systemic inflammation^{3,17}. These findings highlight the importance of investigating regional adiposity and its varied contributions to brain function, underscoring the need for more nuanced research into how regional adiposity influences brain aging and cognitive decline.

This study aimed to investigate the relationship between regional adiposity and brain health in adults, using a large, population-based sample in the UK Biobank¹⁸. Although BMI is commonly used to assess general obesity, it does not capture the unique effects of adiposity across different body regions. We hypothesize that, beyond general obesity, regional adiposity exhibits both shared and differential associations with brain health markers, including brain morphology, functional connectivity (FC) and white-matter microstructure. These associations may contribute to cognitive decline via system-specific patterns of brain aging. To test this, we used dual-energy X-ray absorptiometry (DXA) to quantify adiposity in the arms, trunk, legs and VAT. Brain health was evaluated through multimodal imaging, including measures of brain morphology, FC and white-matter microstructure. We also applied brain age prediction models to estimate system-specific brain age gaps (BAGs), providing insights into how different brain networks may be differentially affected by adiposity. Finally, mediation analyses were used to explore whether brain aging mediates the relationship between regional adiposity and cognitive function (Fig. 1). By integrating these multi-level analyses, this study aims to uncover the heterogeneous effects of regional adiposity on brain aging and cognitive decline, offering new perspectives on the role of regional adiposity in brain health.

Results

Participant characteristics

Regional adiposity measures, including arm fat percentage (AFP), leg fat percentage (LFP) and trunk fat percentage (TFP), were available for 47,764 participants, and VAT was assessed in 40,072 participants in the UK Biobank study. To examine the relationships between these adiposity measures and brain imaging metrics in a non-clinical adult sample, we also selected participants with multimodal brain magnetic resonance imaging (MRI) data and excluded those with major physical, neurological or psychiatric diseases (Supplementary Fig. 1). Consequently, the study included 23,088 participants with AFP, LFP and TFP measurements and 18,886 participants with VAT measurements. Table 1 summarizes the demographic characteristics of the two samples, which were comparable in terms of ethnicity, handedness, unemployment rates, smoking status and alcohol consumption.

Associations of regional adiposity with brain morphology

We first applied a two-step regression approach (Methods) to assess associations between regional adiposity and brain morphology, focusing on both cortical and subcortical structures. Linear regression models, adjusted for a predefined set of covariates, including BMI, age and gender (Methods), were used to identify patterns linking regional adiposity measures to variations in BMI-adjusted morphological metrics. Specifically, higher AFP, TFP and LFP were associated with reductions in cortical volume and surface area in the following regions: (1) the medial prefrontal cortex, posterior cingulate gyrus, precuneus and lateral temporal cortex, which are commonly associated with the default mode network¹⁹ (DMN; Fig. 2a–c, random field theory (RFT) corrected $P_{\text{RFT}} < 2 \times 10^{-16}$); (2) the medial temporal cortex and orbitofrontal cortex (Fig. 2a–c, $P_{\text{RFT}} \leq 4.3 \times 10^{-6}$), which are related to the limbic system. Moreover, higher AFP and TFP were linked to decreased cortical thickness in the sensorimotor cortex (Fig. 2a,b, $P_{\text{RFT}} < 2 \times 10^{-16}$), which was not observed with LFP and VAT. In addition, higher VAT was predominantly associated with a reduction in cortical volume and surface area within the dorsal medial prefrontal cortex and

Table 1 | Demographic characteristics of the selected participants

Characteristics	AFP/LFP/TFP (N=23,088)	VAT (N=18,886)	P value
Age (years)	62.5 (7.40)	62.5 (7.43)	0.80
Male participants	10,444 (45.2%)	8,636 (45.7%)	0.79
Ethnicity			0.60
White	22,259 (96.4%)	18,138 (96.1%)	
Non-white	829 (3.6%)	748 (3.9%)	
Handedness			0.61
Right-handedness	20,526 (88.9%)	16,785 (88.8%)	
Left-handedness	2,562 (11.1%)	2,101 (11.2%)	
Brain size (cm³)	1,193.3 (111.9)	1,195.1 (112.2)	0.11
Years of education (years)	17.7 (4.89)	17.8 (4.88)	0.25
Employment status			0.81
Employed	10,202 (44.1%)	8,365 (44.3%)	
Unemployed	12,886 (55.9%)	10,521 (55.7%)	
Smoking frequency			0.35
Never	22,282 (96.6%)	18,217 (96.4%)	
Occasionally	453 (1.9%)	377 (2.0%)	
Most or all days	353 (1.5%)	292 (1.6%)	
Alcohol consumption frequency			0.34
Never	1,438 (6.2%)	1,143 (6.1%)	
Occasionally	2,288 (9.9%)	1,858 (9.8%)	
Most or all days	2,698 (11.6%)	2,211 (11.7%)	
Once or twice a week	3,767 (16.3%)	3,110 (16.4%)	
Three or four times a week	6,286 (27.2%)	5,128 (27.1%)	
Daily or almost daily	6,611 (28.8%)	5,436 (28.9%)	
Physical activity			0.62
Low	11,667 (50.5%)	9,544 (50.3%)	
Moderate	7,785 (33.7%)	6,358 (33.9%)	
High	3,636 (15.7%)	2,984 (15.8%)	
MetS score	1.76 (0.91)	1.77 (0.92)	0.32
Imaging site			0.77
Cheadle	14,965 (64.8%)	13,856 (73.3%)	
Reading	3,318 (14.4%)	3,301 (17.5%)	
Newcastle	4,805 (20.8%)	1,729 (9.2%)	

Values are presented as mean (s.d.) or number (%). The two-sided Mann–Whitney U test and χ^2 test were used for continuous and categorical variables, respectively. MetS, metabolic syndrome.

precuneus (Fig. 2d, $P_{\text{RFT}} < 2 \times 10^{-16}$), which are the DMN hubs. Furthermore, all four adiposity measures demonstrated significant negative associations with subcortical volumes (Fig. 2a–d, false discovery rate (FDR)-corrected $P_{\text{FDR}} \leq 8.3 \times 10^{-3}$; Supplementary Table 1).

In summary, the fat accumulation in different regions was associated with atrophic changes in brain morphology, characterized by the relatively homogeneous patterns of subcortical atrophy and the heterogeneous patterns of cortical atrophy.

Association of regional adiposity with whole-brain functional connectivity

Two-step linear regression models were also used to explore the associations between regional adiposity and BMI-adjusted FC, adjusting for

the same covariates (Methods). All four regional adiposity measures consistently showed negative associations with FC in the sensorimotor network (SMN) and subcortical–cerebellar–brainstem (SUB-CER-BST) circuits (Fig. 3a–d, $P_{\text{FDR}} \leq 9.3 \times 10^{-3}$). Notably, LFP displayed a strong negative association with FC in the limbic network (LIM; Fig. 3c), while AFP and TFP had weaker associations (Fig. 3a,b, $P_{\text{FDR}} \leq 3.6 \times 10^{-3}$), and VAT showed no significant correlation with LIM FC (Fig. 3d). Additionally, higher AFP, LFP and TFP were associated with increased within-network FC in DMN (Fig. 3a–c, $P_{\text{FDR}} \leq 9.8 \times 10^{-3}$), whereas VAT exhibited no significant association with the DMN connectivity (Fig. 3d). These findings highlight distinct patterns of adiposity-related FC alterations across different brain networks.

Associations of regional adiposity with white-matter microstructure

To investigate the potential impact of regional adiposity on white-matter microstructure, we employed neurite orientation dispersion and density imaging (NODDI). This technique provides detailed insights into white-matter microstructure, particularly focusing on the orientation and density of neurites (axons and dendrites), through three key parameters: neurite density index (NDI), isotropic volume fraction (ISOVF) and orientation dispersion index (ODI)²⁰. Using a two-step regression approach, we found that AFP demonstrated a widespread positive correlation with axon density, as indicated by NDI, in multiple white-matter regions (Fig. 4a), including the bilateral superior longitudinal fasciculus, inferior longitudinal fasciculus, posterior thalamic radiation ($P_{\text{RFT}} \leq 2.2 \times 10^{-6}$), cingulum, anterior corona radiata, external capsule and corpus callosum ($P_{\text{RFT}} \leq 9.8 \times 10^{-9}$). Conversely, AFP was negatively correlated with free water contamination, as indicated by ISOVF, in several regions (Fig. 4a), including the bilateral posterior thalamic radiation, inferior longitudinal fasciculus ($P_{\text{RFT}} \leq 4.0 \times 10^{-8}$), cerebellar peduncles ($P_{\text{RFT}} \leq 3.3 \times 10^{-12}$) and left hippocampus ($P_{\text{RFT}} = 3.5 \times 10^{-9}$). AFP was also positively correlated with ISOVF in the right internal capsule and superior longitudinal fasciculus ($P_{\text{RFT}} = 1.2 \times 10^{-8}$). Additionally, AFP showed positive correlations with axonal organization (Fig. 4a), as indicated by ODI, in the bilateral internal capsules ($P_{\text{RFT}} \leq 3.2 \times 10^{-12}$) and cerebellar peduncles ($P_{\text{RFT}} \leq 1.1 \times 10^{-16}$). TFP exhibited similar relationships with axon density, free water contamination and axonal organization, as well as a similar distribution of affected white-matter regions (Fig. 4b).

LFP displayed fewer significant associations with specific white-matter regions. LFP was positively correlated with axon density (NDI) in the corticospinal tract (Fig. 4c, $P_{\text{RFT}} = 1.5 \times 10^{-7}$) and showed mixed associations with free water contamination (ISOVF; Fig. 4c), including positive correlations in the right superior longitudinal fasciculus, internal capsule ($P_{\text{RFT}} \leq 3.9 \times 10^{-15}$), left anterior corona radiata ($P_{\text{RFT}} = 1.5 \times 10^{-6}$) and corticospinal tract ($P_{\text{RFT}} = 1.9 \times 10^{-10}$), but negative correlations in the left cerebellar peduncle ($P_{\text{RFT}} = 1.1 \times 10^{-16}$) and bilateral hippocampus ($P_{\text{RFT}} \leq 2.2 \times 10^{-7}$). For axonal organization (ODI; Fig. 4c), LFP exhibited positive correlations in the bilateral internal capsules ($P_{\text{RFT}} \leq 3.4 \times 10^{-10}$) and posterior cerebellar peduncles ($P_{\text{RFT}} \leq 7.1 \times 10^{-9}$), alongside negative correlations in the right retro lenticular part of the internal capsule ($P_{\text{RFT}} = 4.6 \times 10^{-10}$) and anterior cerebellar peduncles ($P_{\text{RFT}} = 9.1 \times 10^{-9}$).

VAT had the highest impact on white-matter microstructure among regional adiposity measures. VAT showed negative correlations with axon density (NDI; Fig. 4d) in the bilateral anterior and superior corona radiata, internal capsules, corpus callosum ($P_{\text{RFT}} \leq 3.8 \times 10^{-7}$) and cingulum ($P_{\text{RFT}} = 5.4 \times 10^{-5}$). Positive correlations with free water contamination (ISOVF; Fig. 4d) were observed in extensive white-matter regions, including the bilateral anterior and superior corona radiata, superior longitudinal fasciculus, internal and external capsules, corpus callosum ($P_{\text{RFT}} \leq 6.6 \times 10^{-15}$), cerebral peduncles ($P_{\text{RFT}} \leq 1.0 \times 10^{-10}$) and cerebellar peduncles ($P_{\text{RFT}} \leq 7.0 \times 10^{-11}$). Additionally, VAT exhibited negative correlations with axonal organization (ODI; Fig. 4d) in the

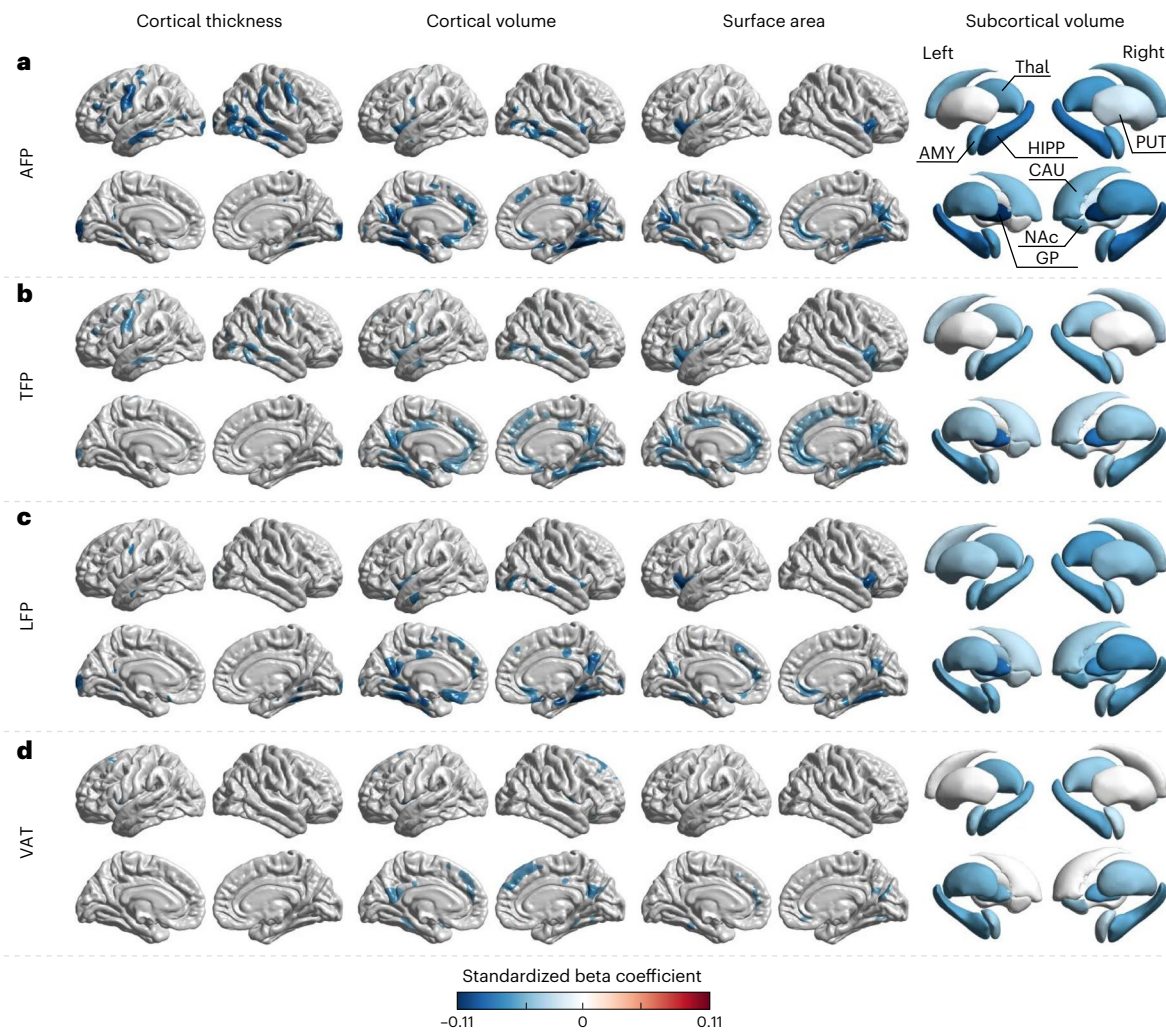


Fig. 2 | Associations of regional adiposity with cortical and subcortical morphometry. **a–d**, The relationships between specific adiposity (**a**, AFP; **b**, TFP; **c**, LFP; **d**, VAT) and brain morphology, with each column representing a morphological parameter: cortical thickness, cortical volume, surface area and subcortical volume (from left to right). The color bar represents standardized beta coefficients, with cooler colors (blue) indicating negative correlations. One-sided linear regression models were used to examine the associations between regional adiposity measures and BMI-adjusted cortical and subcortical metrics, adjusting for age at imaging visit, sex, ethnicity, handedness, years of education,

employment status, smoking frequency, alcohol consumption frequency, physical activity, metabolic syndrome score, brain size and imaging site. For cortical morphological analysis, random field theory was applied to correct for multiple comparisons at a vertex-level threshold of $P < 0.001$ and a cluster-level threshold of $P < 0.01$. FDR was used to correct for multiple comparisons among subcortical volumes at a threshold of $P < 0.01$. AMY, amygdala; CAU, caudate; HIPP, hippocampus; GP, globus pallidus; NAc, nucleus accumbens; PUT, putamen; Thal, thalamus.

bilateral internal and external capsules ($P_{\text{RFT}} \leq 3.1 \times 10^{-7}$), as well as superior corona radiata, cingulum ($P_{\text{RFT}} \leq 3.1 \times 10^{-7}$) and corpus callosum ($P_{\text{RFT}} = 3.7 \times 10^{-12}$).

These results underscore distinct, region-specific relationships between regional adiposity and white-matter microstructure. VAT was associated with compromised white-matter integrity, as evidenced by its correlation with reduced axon density, increased free water contamination and decreased axonal organization. This potentially indicates white-matter fiber degeneration (for example, reduced axonal density) or tissue disorganization. By contrast, AFP, TFP and LFP exhibited less pronounced associations with white-matter integrity.

BMI adjustment reveals distinct associations between regional adiposity and the brain

To contrast BMI-dependent and BMI-independent effects of regional adiposity, we conducted secondary analyses examining the associations of BMI and regional adiposity measures with brain imaging metrics. Before BMI adjustment, regional adiposity exhibited widespread

associations with brain morphology, functional connectivity and white-matter microstructure (panels a–d in Supplementary Figs. 2–4; corrected $P < 0.01$). These patterns closely resembled those observed for BMI (panels e in Supplementary Figs. 2–4), making it difficult to distinguish the specific contribution of regional adiposity. These results suggest that regional adiposity measures may largely act as proxies for general adiposity (that is, BMI) in unadjusted models.

After adjusting for BMI using a two-step regression approach (Methods), the pattern of associations between regional adiposity measures and brain imaging metrics changed substantially. At the brain system level, associations became more spatially localized, primarily converging in the subcortical–cerebellar–brainstem, sensorimotor, limbic and default mode systems. The overall strength of these associations was attenuated, and in multiple subcortical structures (for example, the putamen, amygdala and thalamus), the direction of association reversed from positive to negative. These findings highlight a potential masking effect of BMI, whereby shared variance may obscure associations between regional adiposity and brain metrics. By disentangling

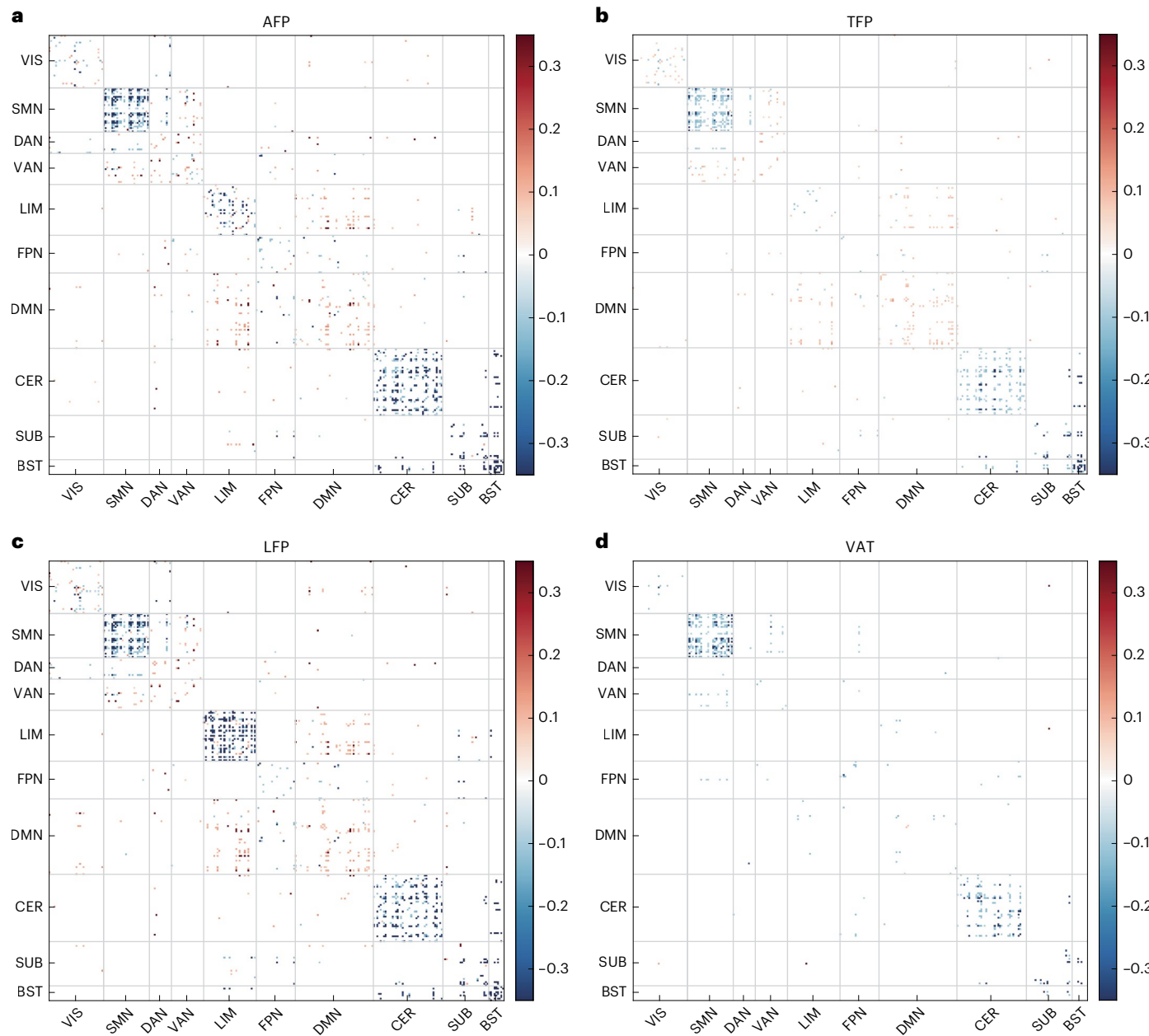


Fig. 3 | Associations of regional adiposity with functional connectivity. **a–d**, Functional connections significantly associated with regional adiposity (**a**, AFP; **b**, TFP; **c**, LFP; **d**, VAT). The color bar represents standardized beta coefficients, with warmer colors (red) indicating positive correlations and cooler colors (blue) indicating negative correlations. Two-sided linear regression models were used to examine the associations between regional adiposity measures and BMI-adjusted functional connectivity, adjusting for age at

imaging visit, sex, ethnicity, handedness, years of education, employment status, smoking frequency, alcohol consumption frequency, physical activity, metabolic syndrome score, brain size and imaging site. Statistical significance was determined using FDR correction at a threshold of $P < 0.01$. VIS, visual network; DAN, dorsal attention network; VAN, ventral attention network; FPN, frontoparietal network; DMN, default mode network; CER, cerebellar network; SUB, subcortical network; BST, brainstem network.

these effects, our analytical framework reveals that regional adiposity is associated with distinct patterns of brain morphology, connectivity and microstructure that are not accounted for by BMI, reinforcing its added value in understanding obesity-related brain variation.

Associations between regional adiposity, brain age and cognitive function

We further investigated whether brain regions affected by regional adiposity mediated the relationship between regional adiposity and cognitive function. For this, the system-specific BAG was estimated based on the features of specific brain systems defined in Figs. 2–4 via partial least squares (Methods and Supplementary Fig. 5).

The mediation results, detailed in Supplementary Tables 2–4, revealed that BAGs derived from the sensorimotor, limbic and default mode systems significantly mediated the relationships between regional adiposity and cognitive functions, including reasoning, executive function, processing speed and memory ($P_{\text{FDR}} < 9.8 \times 10^{-3}$). By contrast, the BAG derived from the subcortical–cerebellar–brainstem system did not significantly mediate these relationships (Supplementary Tables 5; $P_{\text{FDR}} > 0.01$). Notably, the strongest indirect effects were observed in the mediation of the relationship between VAT and cognition (Fig. 5 and Supplementary Tables 2–5). These findings suggest that cortical-related BAGs play a significant role in mediating the impact of regional adiposity on cognitive functions, with VAT exerting the most pronounced effect.

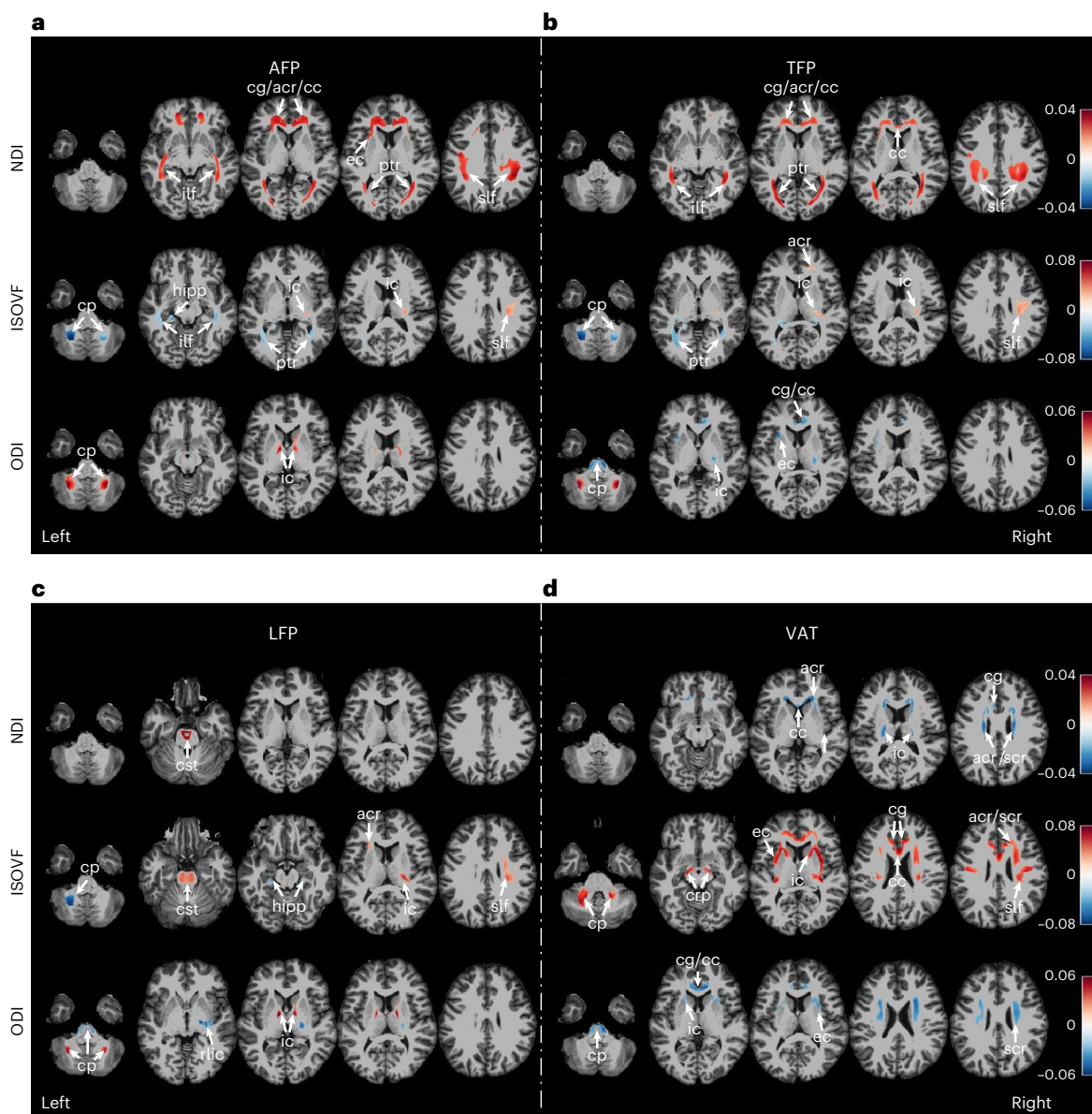


Fig. 4 | Association of fat distribution with NODDI metrics. **a–d**, The relationship between fat distribution (**a**, AFP; **b**, TFP; **c**, LFP; **d**, VAT) and three key NODDI metrics: ICVF, ISOVF and ODI. Regions with significant associations are highlighted, with warm colors (red) indicating positive correlations and cool colors (blue) indicating negative correlations, represented by standardized beta coefficients. Two-sided linear regression models were used to examine the associations between regional adiposity measures and BMI-adjusted NODDI metrics, adjusting for age at imaging visit, sex, ethnicity, handedness, years of education, employment status, smoking frequency, alcohol consumption

frequency, physical activity, metabolic syndrome score, brain size and imaging site. Statistical significance was determined using random field theory correction with a voxel-level threshold of $P < 0.001$ and a cluster-level threshold of $P < 0.01$. slf, superior longitudinal fasciculus; ilf, inferior longitudinal fasciculus; ptr, posterior thalamic radiation; arc, anterior corona radiata; src, superior corona radiata; cg, cingulum; cc, corpus callosum; ec, external capsule; ic, internal capsule; rlic, retro lenticular part of the internal capsule; hippocampus; cp, cerebellar peduncle; crp, cerebral peduncle.

Discussion

This study leveraged DXA and brain imaging data from the UK Biobank study to comprehensively investigate the relationships between regional adiposity and brain health. Our analyses revealed that adiposity in the arm, trunk, leg and visceral regions was differentially associated with brain imaging metrics, with spatial patterns predominantly involving the subcortical–cerebellar–brainstem, sensorimotor, limbic and default mode systems. Importantly, these associations were independent of general obesity, as each regional adiposity measure was statistically modeled to exclude variance shared with BMI. Furthermore, BAGs derived from the sensorimotor, limbic and default mode systems significantly mediated the relationships between regional

adiposity and cognitive performance. These findings suggest that the accumulation of regional adiposity may contribute to cognitive decline by accelerating system-specific patterns of brain aging. Among all regional adiposity measures, visceral adiposity demonstrated the strongest negative associations with both brain integrity and cognitive function, highlighting its potential role as a critical marker of obesity-related neurocognitive risk.

Although BMI remains the most widely used index of obesity, it often obscures the distinct contributions of regional fat distribution to health outcomes^{21–23}. In the present study we employed a two-step regression approach to first remove the effects of BMI, allowing us to more accurately assess the associations between regional adiposity

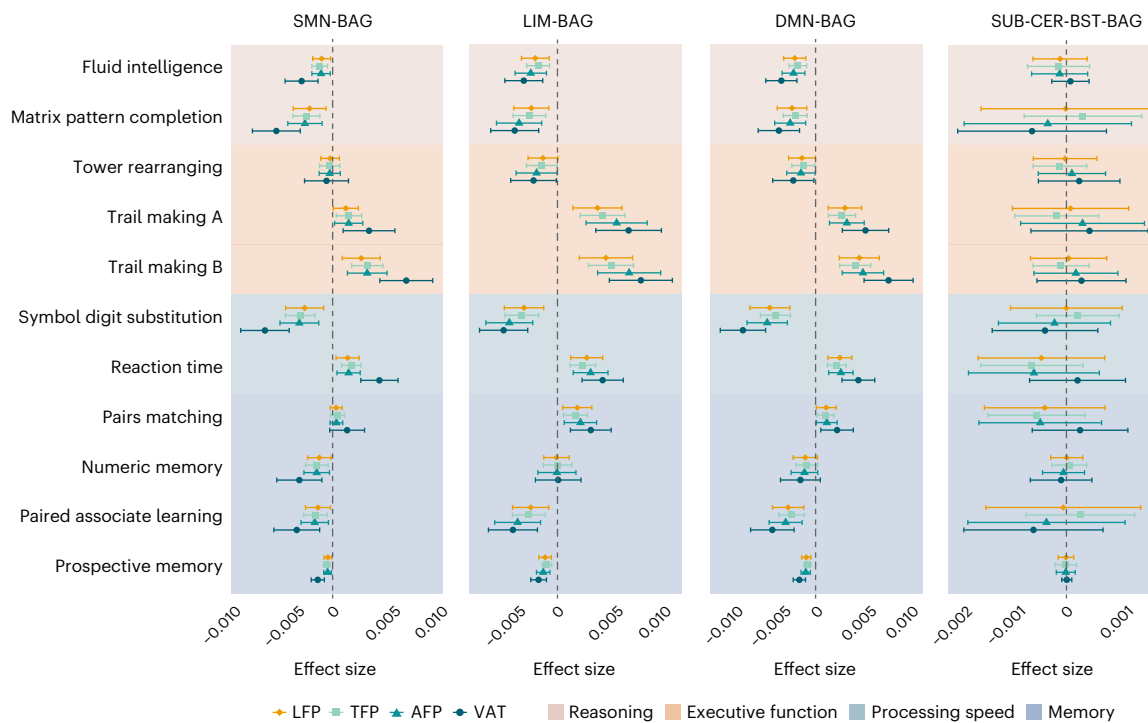


Fig. 5 | Indirect effects of system-specific BAGs on the relationship between regional adiposity and cognitive function. Forest plots are presented that illustrate the indirect effect sizes (points) along with their 95% bias-corrected confidence intervals (horizontal bars), derived from two-sided mediation analyses with 5,000 bootstrap iterations. All models were adjusted for age at imaging visit, sex, ethnicity, handedness, years of education, employment status, smoking frequency, alcohol consumption frequency, physical activity, metabolic syndrome score, brain size and imaging site. Sample sizes varied across cognitive

tests due to differences in data availability, ranging from approximately 15,057 to 21,867 participants per model (Supplementary Tables 2–4). BAGs derived from the sensorimotor network (SMN-BAG), limbic (LIM-BAG) and default mode (DMN-BAG) systems broadly mediated the relationships between regional adiposity and cognitive function (FDR-corrected $P < 0.01$). By contrast, the BAG derived from the subcortical–cerebellar–brainstem circuits (SUB-CER-BST-BAG) system did not exhibit a significant indirect effect ($P_{\text{FDR}} > 0.01$).

and brain imaging metrics. Their associations became more spatially localized within four key brain systems. For several subcortical regions, such as the putamen, amygdala and thalamus, we observed a reversal in the direction of association from positive to negative, likely reflecting a masking effect arising from shared variance between BMI and regional adiposity²⁴. The relative homogeneity of associations observed between regional adiposity and subcortical structures may help reconcile inconsistencies reported in previous studies regarding the relationship between obesity and subcortical volumes^{25–27}. These findings highlight the importance of examining regional adiposity independently of BMI to reveal more specific and reliable associations with brain health.

In the present study, four brain systems, including the subcortical–cerebellar–brainstem, sensorimotor, limbic and default mode systems, were most commonly implicated in relation to regional adiposity. These systems are known to support homeostatic regulation, motor control, emotional processing and self-referential cognition^{28–35}, and are frequently involved in obesity-related neural alterations. Typically, the subcortical–cerebellar–brainstem system is particularly relevant to homeostatic function. The hypothalamus and the brainstem-located nucleus of the solitary tract are well-established regulators of homeostatic processes, including appetite, energy balance and autonomic control^{36–38}. Although our analysis did not detect direct associations with these nuclei, previous studies have demonstrated that subcortical and cerebellar regions are closely connected to them both anatomically and functionally^{39,40}. These findings suggest that regional adiposity may be particularly informative for identifying core neural alterations commonly observed in obesity-related brain changes. However, the spatial distribution of these associations did not fully align across imaging modalities. For example, the default mode system showed structural

atrophy in key hubs such as the precuneus and medial prefrontal cortex, in association with visceral adiposity, without corresponding reductions in functional connectivity. These divergences may reflect differences in temporal sensitivity across imaging techniques, where structural degeneration may precede measurable functional impairments^{41,42}, or compensatory plasticity may help preserve connectivity in vulnerable systems⁴³. Furthermore, the intrinsic nature of resting-state fMRI may limit its ability to detect subtle or task-dependent disruptions that emerge under cognitive or metabolic challenges⁴⁴. Together, these insights highlight that combining multimodal MRI with detailed regional adiposity measures may offer a more precise and comprehensive view of the brain–fat connection.

Our findings also revealed differential associations between specific adiposity regions and brain imaging metrics. Specifically, adiposity in the arm and trunk showed more pronounced associations with cortical thinning in the sensorimotor cortex compared to leg and visceral regions. This pattern aligns with earlier evidence suggesting that upper-body adiposity may exert greater metabolic and cardiovascular burden than lower-body adiposity^{45,46}. Importantly, the sensorimotor cortex is vulnerable to age-related atrophy^{47,48}, which may be partly attributable to its high metabolic activity⁴⁹. Moreover, we observed a consistent negative association between arm adiposity and hippocampal volume, both before and after adjusting for BMI (Fig. 2a and Supplementary Fig. 2a). The hippocampus is a key region for memory processing and a critical structure implicated in Alzheimer's disease. This association suggests a degree of specificity in the link between upper-body fat accumulation and memory decline, potentially offering a neurostructural explanation for the elevated Alzheimer's disease risk associated with greater upper-body adiposity³. Declines in sensorimotor and cognitive functions are hallmarks of healthy aging⁵⁰.

The associations we observed between upper-body adiposity and brain regions involved in sensorimotor and cognitive functions may point to its potential role in shaping brain aging trajectories. While the causal nature of these associations remains to be clarified, our findings highlight a plausible link that merits deeper exploration.

In contrast, adiposity in the leg was associated with more pronounced reductions in functional connectivity within the limbic system, a system critically involved in emotional regulation, memory, and reward processing⁵¹. Lower-body adiposity is often considered protective for metabolic health⁵², but its effects on brain function appear more complex. One speculative but biologically plausible explanation involves leptin signaling. Previous studies suggest that lower-body adipose tissue may secrete leptin at higher rates compared to upper-body fat depots⁵³. Moreover, leptin receptors are expressed in several limbic regions, including the hippocampus, where leptin modulates synaptic plasticity, neurogenesis and neural circuits involved in memory regulation^{54,55}. Although our study did not directly assess leptin levels, previous work has shown that elevated circulating leptin may be associated with functional connectivity reductions in the limbic system⁵⁶. Taken together, these findings raise the possibility that leptin-related pathways may contribute to the observed associations between leg adiposity and limbic dysfunction. Further research is needed to directly test this hypothesis.

Moreover, visceral adiposity demonstrated a stronger association with white-matter microstructural abnormalities in our study, characterized by reduced axon density and tissue degeneration, whereas adiposity in the arm, trunk and leg was linked to preserved white-matter integrity. This apparent paradox may be explained by differences in inflammatory responses: visceral adipose tissue secretes pro-inflammatory factors (for example, TNF- α), triggering systemic inflammation that contributes to neuroinflammation and white-matter damage^{53,57}. In contrast, adiposity in the arms, trunk and legs exhibits lower levels of inflammatory factor secretion, potentially supporting synaptic plasticity and neurite density within physiological ranges⁵⁸. Collectively, these findings highlight the distinct effects of regional adiposity on brain health, with visceral adipose exhibiting the strongest negative associations across regional adiposity, likely due to its unique pro-inflammatory profile.

Our results demonstrated that the BAGs derived from the sensorimotor, limbic and default mode systems, rather than from the subcortical–cerebellar–brainstem system, mediate the relationships between regional adiposity and cognitive performance in reasoning, executive function, processing speed and memory. These cognitive domains are crucial to healthy aging⁵⁹ and are closely linked to the functions of the frontal, parietal and temporal cortical regions^{60–62}, which plausibly supports that regional adiposity may contribute to cortical brain aging and subsequent cognitive decline. Moreover, among the four adiposity measures examined, visceral adiposity consistently exhibited the strongest indirect effects on cognition via these cortical BAGs. Taken together, these findings underscore both the system-specific vulnerabilities to regional adiposity-related brain aging and the disproportionate neurocognitive burden associated with fat distributed in different body regions, reflecting several clinically relevant implications. First, the consistent mediating roles of cortical-system BAGs highlight their potential utility in identifying individuals whose cognitive performance may be particularly vulnerable to excess adiposity. Second, the disproportionate effects of visceral adiposity across all cognitive domains underscore its relevance as a key intervention target, supporting the notion that visceral fat is strongly associated with neurodegeneration⁶³. Clinical strategies aimed at reducing visceral adiposity, whether through lifestyle modification or pharmacologic means, may help slow cognitive aging in at-risk obese populations.

The strengths of this study include its large sample size, the use of multimodal neuroimaging, and quantitative analysis of regional adiposity across multiple regions, providing a robust framework for

understanding the unique contributions of fat distribution to brain health. However, several limitations should be noted. First, the cross-sectional design limits causal inferences between regional adiposity and brain health. Longitudinal studies are needed to determine whether fat accumulation drives changes in brain structure and function or vice versa. Second, although DXA provides a reliable measure of regional adiposity, it lacks the resolution to differentiate subcutaneous fat from visceral fat within the trunk, potentially limiting insights into their distinct effects. Third, the sample population may be relatively biased in terms of ethnicity, lifestyle and socioeconomic background, which may limit the generalizability of our findings to more diverse populations. Replication in broader demographic settings is warranted. Last, but not least, the potential moderating role of sex was not directly examined in this study, although our models adjusted for sex. Given well-established differences in fat distribution and brain-aging trajectories between male and female participants^{64,65}, future studies should consider sex-stratified analyses to better understand whether and how regional adiposity impacts brain aging and cognition differently by sex. Investigating these interactions may reveal sex-specific neurobiological pathways and enhance the precision of intervention strategies.

In conclusion, this study provides a comprehensive framework to delineate the differential relationships between regional adiposity and the selective vulnerability of brain systems and cognitive function. By integrating multimodal brain imaging with regional adiposity measures, our work offers a novel perspective on the link between regional adiposity and obesity-related brain alterations, although the effect sizes are modest. It also underscores the heterogeneous nature of the brain–fat connection and the potential role of regional adiposity, particularly visceral adiposity, in shaping trajectories of brain and cognitive aging.

Together, this work strengthens the rationale for incorporating regional adiposity into future neuro-epidemiological research and highlights its potential to inform strategies preserving brain health. However, given the cross-sectional nature of this study, causal inferences cannot be drawn. Longitudinal and interventional studies are warranted to further evaluate the predictive utility of these markers and their relevance to trajectories of neurocognitive aging.

Methods

Participants

We analyzed data from the UK Biobank (application no. 57831), a nationwide population cohort that enrolled more than 500,000 adults at assessment centers across the United Kingdom between 2006 and 2010. The present analyses were conducted under the ethical approval granted to the UK Biobank by the UK National Health Service National Research Ethics Service (reference 11/NW/0382). All participants provided written informed consent and were allowed to withdraw at any time without explanation. Study-related risk was considered minimal. However, UK Biobank maintains insurance arrangements that provide compensation for injuries arising from negligent conduct during participation.

This study leveraged publicly accessible demographic, phenotypic, image and cognitive data from the UK Biobank, ensuring compliance with its ethical and data access guidelines. A detailed flowchart of participant selection is provided in Supplementary Fig. 1. During the first imaging visit, both DXA and brain MRI examinations were conducted. For this study, we identified 47,764 participants with available AFP, TFP and LFP data and 40,072 participants with VAT measurements. We excluded participants who had major physical, neurological or psychiatric disorders (Supplementary Methods)⁶⁶, as well as those whose MRI scans did not meet quality standards. This resulted in analytic samples of 23,088 participants (mean age = 62.5 ± 7.40 years (s.d.); 45.2% male participants) and 18,886 participants (mean age = 62.5 ± 7.43 years (s.d.); 45.7% male participants) for fat percentage and VAT analyses, respectively. These analyses aimed to investigate the associations between regional adiposity measures and brain imaging metrics. Furthermore, participants who underwent cognitive function assessments

at the assessment centers were selected to explore the relationships among regional adiposity, brain aging and cognitive performance.

Regional adiposity

Body regional adiposity was assessed during the first imaging visit by DXA with an iDXA instrument (GE-Lunar). The instrument underwent daily calibration using the manufacturer-provided phantom and routine quality-control procedures to ensure measurement accuracy. Whole-body scans were conducted with participants positioned supine on the DXA couch. Four DXA-derived measures (AFP, TFP, LFP and VAT) were selected as regional adiposity indicators across the arm, trunk, leg and VAT. Specifically, 'arms' included the arms and shoulders, 'trunk' encompassed the neck, chest, abdomen and pelvis, and 'legs' referred to all areas below the trunk. VAT was assessed as the tissue mass (grams) of VAT, estimated using an established model based on DXA data⁶⁷.

Anthropometric data were collected during the same assessment visit by trained clinic staff, following the UK Biobank standardized protocol⁶⁸. Body weight was obtained using a Tanita BC-418 MA body composition analyzer (Tanita Corporation), and standing height was measured with a wall-mounted Seca 240 stadiometer (Seca). BMI, as a general obesity measure, was calculated as weight in kilograms divided by height in meters squared. The complete UK Biobank anthropometric protocol is publicly available online (<https://biobank.ndph.ox.ac.uk/showcase/refer.cgi?id=146620>).

Multimodal brain imaging

Multimodal brain MRI data, including structural T1-weighted MRI, resting-state functional MRI (rs-fMRI) and diffusion-weighted imaging (DWI), were obtained from the UK Biobank repository. These MRI scans were originally collected during the second follow-up visit (that is, first imaging visit) at three designated centers (Cheadle, Newcastle and Reading) using consistent acquisition protocols on Siemens Skyra 3T scanners with 32-channel head coils. The complete imaging protocol is publicly available online (<http://biobank.ctsu.ox.ac.uk/crystal/refer.cgi?id=2367>)⁶⁹. In the present study, we processed these existing raw MRI data to derive brain imaging metrics for analysis.

Structural T1-weighted MRI. T1-weighted MRI underwent quality control and preprocessing using FreeSurfer (version 7.1.1)⁷⁰. For cortical thickness, volume and surface area, vertex-wise registration to the template was followed by smoothing with a 10-mm full-width at half-maximum Gaussian kernel, which increases signal-to-noise ratios and reduces misregistration artifacts⁶⁶. Subcortical volumes were derived by FreeSurfer automated segmentation⁷⁰, including the bilateral nucleus accumbens, caudate nucleus, putamen, globus pallidus, thalamus, hippocampus and amygdala.

Rs-fMRI. The rs-fMRI data were preprocessed using a standardized pipeline (detailed steps are provided in the Supplementary Methods). FC was assessed by calculating Pearson's correlation coefficients between all pairs of 268 regions of interest defined in Shen's atlas⁷¹, and the resulting coefficients were Fisher z-transformed. To account for the sparse nature of human brain connectivity^{72–74}, the strongest 10% of connections were empirically selected for subsequent analysis^{75,76}. This proportional threshold enhances the robustness of cross-subject comparisons while minimizing spurious connectivity. For network-level analysis, the 268 regions of interest were organized into ten functional networks, including Yeo's seven networks⁷⁷ and SUB-CER-BST circuits: visual (VIS), SMN, dorsal attention (DAN), ventral attention (VAN), LIM, frontoparietal (FPN), DMN, CER, SUB and BST.

DWI. This study utilized the NODDI model to analyze DWI data, generating meaningful voxel-wise microstructural parameters, including NDI (an index of white-matter neurite density), ISOVF (an index of free water content) and ODI (an index of variability in fiber orientations)²⁰. NODDI

was chosen over conventional diffusion tensor imaging (DTI) for its ability to capture complex microstructural properties, such as neurite density and orientation dispersion. Unlike DTI, which assumes Gaussian diffusion and is limited to basic metrics such as fractional anisotropy and mean diffusivity, NODDI provides greater specificity and sensitivity, particularly in detecting subtle changes in heterogeneous brain regions. Preprocessing for diffusion imaging included correction for eddy currents and head motion, removal of outlier slices, and NODDI model fitting using the AMICO pipeline⁷⁸. The preprocessing pipeline for DWI brain imaging data is described in the Supplementary Methods.

Cognitive functions

Cognitive performance was assessed using a series of well-established, touchscreen-based tasks in the second follow-up visit⁷⁹. These tasks were designed to comprehensively evaluate distinct cognitive functions, including reasoning, executive function, processing speed and memory. The test procedures and measurements are described in Supplementary Table 6.

Reasoning ability was assessed using the fluid intelligence test (FIT) and the matrix pattern test (MPT). In the FIT, participants responded to 13 questions within 2 min, with performance measured as the unweighted sum of correct answers. The MPT required participants to identify missing elements in a visual matrix, with scores based on the number of puzzles for which the correct solution was provided.

Executive function was assessed using the trail making test (TMT) and the tower rearranging test (TRT). The TMT consists of two parts. Part A (TMTA) required participants to connect a sequence of numbered circles as quickly as possible. Part B (TMTB) extended this task by requiring participants to alternate between numbers and letters (for example, 1-A-2-B). Performance in both parts was assessed by completion time. The TRT involved rearranging blocks under specific constraints, with performance measured by the total number of correctly completed puzzles.

Processing speed was assessed using the symbol digit test (SDT) and the reaction time test (RTT). The SDT required participants to match symbols to corresponding digits within a time limit, with performance measured by the number of correct matches. The RTT assessed motor response speed to visual stimuli across nine trials, with results reported as the mean response time.

Memory tasks targeted various memory processes, including working memory, declarative memory and prospective memory. Working memory capacity was evaluated using the numeric memory test (NMT), where participants recalled sequences of increasing length, with performance recorded as the maximum sequence correctly recalled. The pairs matching test (PairsMT) assessed visual declarative memory by requiring participants to recall previously displayed pairs of cards, with performance measured by the number of correct associations. The paired associate learning test (PALT) assessed verbal declarative memory by evaluating participants' ability to recall item pairs after an initial learning phase, with performance measured by the number of correct responses. Finally, prospective memory was assessed using the prospective memory test (PMT), where participants were instructed to recall specific actions after a delay, with performance recorded as a binary outcome (success or failure).

In these cognitive tasks, higher scores on the TMTA, TMTB, PairsMT and RTT indicate poorer performance, whereas higher scores on the other tests reflect better cognitive performance.

Covariates

In this study, covariates were selected based on their potential associations with obesity and brain characteristics, as reported in previous research^{66,80}. Age at the time of the imaging visit (the second follow-up wave) was included as a covariate. Additional baseline covariates encompassed demographics (sex, ethnicity and handedness), socio-economic status (years of education and employment status), lifestyle

factors (physical activity, smoking frequency and alcohol consumption frequency) and metabolic health, represented by the metabolic syndrome score^{66,80}. At the imaging visit, MRI scanning centers were considered to account for variability in imaging equipment, brain size was included to adjust for differences in brain morphology, and mean framewise displacement was included to control for head motion. Imaging sites (Cheadle, Reading and Newcastle) were also included as a covariate to control potential differences due to scanner variability. More details are provided in the Supplementary Methods.

Statistical analyses

Demographic and phenotypic characteristics were compared across samples using the Mann–Whitney U test for continuous variables and the χ^2 test for categorical variables, as described in our previous work^{66,80}. Analyses were conducted in R (version 4.3.1) and Python (version 3.6), with statistical significance defined as a two-sided $P < 0.01$.

Given the high collinearity between regional adiposity measures and BMI, we first adopted a two-step regression approach to isolate the specific associations between regional adiposity and brain imaging metrics. In the initial step, each brain imaging metric was regressed on BMI. The resulting residuals reflected variation in brain imaging metrics not explained by general adiposity. In the second step, we examined whether regional adiposity measures were associated with these residuals, controlling for a set of covariates. This decomposition framework allowed us to estimate associations between regional adiposity and brain structure or function independently of BMI. Before association analyses, regional adiposity measures and brain imaging metrics were z-score standardized, allowing beta coefficients from correlation and mediation models to be interpreted as standardized effect sizes. A directional test (one-sided linear regression) was applied only to cortical metrics, as the earlier literature predominantly supports the hypothesis of obesity-related cortical atrophy^{81–83}. For all other linear regression analyses, two-sided tests were used. For cortical metrics (thickness, volume and surface area), analyses were performed using the SurfStat toolbox (<http://www.math.mcgill.ca/keith/surfstat>), with multiple comparisons corrected using RFT at a cluster threshold of $P < 0.01$ and a vertex-level threshold of $P < 0.001$. Voxel-based analyses for the NODDI parameters were conducted in SPM12 (<https://www.fil.ion.ucl.ac.uk/spm/>), applying RFT correction with the same thresholds (cluster-level, $P < 0.01$; voxel-level, $P < 0.001$). Subcortical structures and FC analysis were analyzed using linear regression in Python (version 3.6), with multiple comparisons addressed by the FDR method ($P_{FDR} < 0.01$). To ensure appropriate control of type I errors, multiple comparisons were corrected separately for each brain imaging metric (for example, cortical thickness, cortical surface area, cortical volume, subcortical volume, FC and each NODDI metric).

In addition to the main analysis, to aid interpretation of the primary models, we conducted secondary analyses in which each adiposity measure (BMI, AFP, LFP, TFP or VAT) was entered separately as a predictor of brain imaging metrics, adjusting for the same covariates as stated above. Each model included only one adiposity measure to avoid adjusting for shared variance across measures. Results are provided in the Supplementary Materials. Together, this two-tiered approach allowed us to systematically disentangle the unique associations of regional adiposity with brain imaging metrics, independent of general obesity.

Considering that the subcortical–cerebellar–brainstem, sensorimotor, limbic and default mode systems were the most frequently reported brain systems that were related to regional adiposity in our study, we developed multimodal brain age prediction models to identify potential system-specific brain age. We utilized multimodal data within each brain system as inputs, encompassing brain morphological, voxel-based NODDI and functional connectivity measures. Specifically, we employed partial least-squares regression, which is well-suited

for handling high-dimensional data, reducing multicollinearity, and extracting latent components that maximize the covariance between predictors and outcomes^{80,84}. An independent partial least-squares model was built for each brain system (details are provided in the Supplementary Methods). Within a stratified tenfold cross-validation, we systematically evaluated models containing 1–20 latent components and retained the dimensionality that minimized the fold-averaged mean absolute error. The optimal dimensionality converged on 13–19 across systems. Tenfold cross-validation was used to compute system-specific BAGs, which were subsequently de-biased for chronological age, where commonly observed as overestimation in younger individuals and underestimation in older individuals^{85,86}. Importantly, chronological age was not regressed out before training, consistent with previous work⁸⁰, to ensure the full variance relevant to age prediction was retained during model fitting. These system-specific BAGs were carried forward to the mediation analyses. The performance of each model is provided in Supplementary Fig. 5. All processes related to model development and the computation of BAGs were implemented in Python (version 3.6).

Finally, we conducted mediation analysis using the ‘lavaan’ package (version 0.6–19) in R (version 4.3.1) with 5,000 bootstrap iterations to assess the indirect effects of system-specific BAGs on the relationship between regional adiposity and cognitive tests. P values were corrected for FDR, with statistical significance set at $P < 0.01$.

Reporting Summary

Further information on research design is available in the Nature Portfolio Reporting Summary linked to this Article.

Data availability

This study utilized data from the UK Biobank, a publicly accessible health research resource. Access to these data requires registration and approval via the UK Biobank application portal (<http://www.ukbiobank.ac.uk/register-apply/>). The dataset includes demographic information, four dual-energy X-ray absorptiometry-derived regional adiposity measures—arm fat percentage, trunk fat percentage, leg fat percentage and visceral adipose tissue—as well as MRI-based brain imaging and cognitive assessments.

Code availability

The study employed linear regression and mediation analysis implemented in MATLAB (2017b; The MathWorks, Inc., USA) and R (version 4.3.1). The code for these two models is available at https://github.com/fuyingji102/regional_adiposity.

References

- Welsh, A., Hammad, M., Piña, I. L. & Kulinski, J. Obesity and cardiovascular health. *Eur. J. Prev. Cardiol.* **31**, 1026–1035 (2024).
- Blüher, M. Obesity: global epidemiology and pathogenesis. *Nat. Rev. Endocrinol.* **15**, 288–298 (2019).
- Xu, S. et al. Association between body composition patterns, cardiovascular disease, and risk of neurodegenerative disease in the UK Biobank. *Neurology* **103**, e209659 (2024).
- Bischof, G. N. & Park, D. C. Obesity and aging: consequences for cognition, brain structure and brain function. *Psychosom. Med.* **77**, 697–709 (2015).
- Xu, X., Xu, Y. & Shi, R. Association between obesity, physical activity, and cognitive decline in Chinese middle and old-aged adults: a mediation analysis. *BMC Geriatr.* **24**, 54 (2024).
- Mina, T. et al. Adiposity impacts cognitive function in Asian populations: an epidemiological and Mendelian Randomization study. *Lancet Reg. Health West Pac.* **33**, 100710 (2023).
- Fernandez-Andujar, M., Morales-Garcia, E. & Garcia-Casares, N. Obesity and gray matter volume assessed by neuroimaging: a systematic review. *Brain Sci.* **11**, 999 (2021).

8. Syan, S. K. et al. Dysregulated resting state functional connectivity and obesity: a systematic review. *Neurosci. Biobehav. Rev.* **131**, 270–292 (2021).
9. Kullmann, S., Schweizer, F., Veit, R., Fritzsche, A. & Preissl, H. Compromised white matter integrity in obesity. *Obes. Rev.* **16**, 273–281 (2015).
10. Dahl, A. K. & Hassing, L. B. Obesity and cognitive aging. *Epidemiol. Rev.* **35**, 22–32 (2013).
11. Loaiza, V. M. An overview of the hallmarks of cognitive aging. *Curr. Opin. Psychol.* **56**, 101784 (2024).
12. Fantuzzi, G. Adipose tissue, adipokines and inflammation. *J. Allergy Clin. Immunol.* **115**, 911–919 (2005).
13. Trayhurn, P. Adipokines: inflammation and the pleiotropic role of white adipose tissue. *Br. J. Nutr.* **127**, 161–164 (2022).
14. Levine, M. E. & Crimmins, E. M. Sarcopenic obesity and cognitive functioning: the mediating roles of insulin resistance and inflammation? *Curr. Gerontol. Geriatr. Res.* **2012**, 826398 (2012).
15. Kwan, P. Sarcopenia, a neurogenic syndrome? *J. Aging Res.* **2013**, 791679 (2013).
16. Low, S. et al. Association between lower extremity skeletal muscle mass and impaired cognitive function in Type 2 Diabetes. *Sci. Rep.* **10**, 2956 (2020).
17. Alser, M. & Elrayess, M. A. From an apple to a pear: moving fat around for reversing insulin resistance. *Int. J. Environ. Res. Public Health* **19**, 14251 (2022).
18. Sudlow, C. et al. UK biobank: an open access resource for identifying the causes of a wide range of complex diseases of middle and old age. *PLoS Med.* **12**, e1001779 (2015).
19. Menon, V. 20 years of the default mode network: a review and synthesis. *Neuron* **111**, 2469–2487 (2023).
20. Zhang, H., Schneider, T., Wheeler-Kingshott, C. A. & Alexander, D. C. NODDI: practical in vivo neurite orientation dispersion and density imaging of the human brain. *NeuroImage* **61**, 1000–1016 (2012).
21. Frank, A. P., de Souza Santos, R., Palmer, B. F. & Clegg, D. J. Determinants of body fat distribution in humans may provide insight about obesity-related health risks. *J. Lipid Res.* **60**, 1710–1719 (2019).
22. Bonora, E. et al. Total body fat content and fat topography are associated differently with in vivo glucose metabolism in nonobese and obese nondiabetic women. *Diabetes* **41**, 1151–1159 (1992).
23. Hotchkiss, J. W. & Leyland, A. H. The relationship between body size and mortality in the linked Scottish Health Surveys: cross-sectional surveys with follow-up. *Int. J. Obes. (Lond.)* **35**, 838–851 (2011).
24. Tu, Y. K., Gunnell, D. & Gilthorpe, M. S. Simpson's Paradox, Lord's Paradox, and Suppression Effects are the same phenomenon—the reversal paradox. *Emerg. Themes Epidemiol.* **5**, 2 (2008).
25. Opel, N. et al. Brain structural abnormalities in obesity: relation to age, genetic risk and common psychiatric disorders: evidence through univariate and multivariate mega-analysis including 6,420 participants from the ENIGMA MDD working group. *Mol. Psychiatry* **26**, 4839–4852 (2021).
26. Janowitz, D. et al. Association between waist circumference and gray matter volume in 2,344 individuals from two adult community-based samples. *NeuroImage* **122**, 149–157 (2015).
27. Kharabian Masouleh, S. et al. Higher body mass index in older adults is associated with lower gray matter volume: implications for memory performance. *Neurobiol. Aging* **40**, 1–10 (2016).
28. Dallman, M. F. Stress-induced obesity and the emotional nervous system. *Trends Endocrinol. Metab.* **21**, 159–165 (2010).
29. Kenny, P. J. Reward mechanisms in obesity: new insights and future directions. *Neuron* **69**, 664–679 (2011).
30. Yoshida, J. et al. Cerebellar contributions to the basal ganglia influence motor coordination, reward processing and movement vigor. *J. Neurosci.* **42**, 8406–8415 (2022).
31. Bruce, K., Garrido, A. N., Zhang, S. Y. & Lam, T. K. T. Regulation of energy and glucose homeostasis by the nucleus of the solitary tract and the area postrema. *Endocrinol. Metab. (Seoul)* **39**, 559–568 (2024).
32. Song, L., Zhang, Y., Chen, T., Maitusong, P. & Lian, X. Association of body perception and dietary weight management behaviours among children and adolescents aged 6–17 years in China: cross-sectional study using CHNS (2015). *BMC Public Health* **22**, 175 (2022).
33. Barros, W. M. A. et al. Effects of overweight/obesity on motor performance in children: a systematic review. *Front. Endocrinol. (Lausanne)* **12**, 759165 (2021).
34. Berthoud, H. R., Munzberg, H. & Morrison, C. D. Blaming the brain for obesity: integration of hedonic and homeostatic mechanisms. *Gastroenterology* **152**, 1728–1738 (2017).
35. Olivo, G. et al. Resting-state brain and the FTO obesity risk allele: default mode, sensorimotor and salience network connectivity underlying different somatosensory integration and reward processing between genotypes. *Front. Hum. Neurosci.* **10**, 52 (2016).
36. Brüning, J. C. & Fenselau, H. Integrative neurocircuits that control metabolism and food intake. *Science* **381**, eabl7398 (2023).
37. Zhang, C. et al. The dorsomedial hypothalamus and nucleus of the solitary tract as key regulators in a rat model of chronic obesity. *Brain Res.* **1727**, 146538 (2020).
38. Berthoud, H. R. & Morrison, C. The brain, appetite and obesity. *Annu. Rev. Psychol.* **59**, 55–92 (2008).
39. Forstenpointner, J. et al. The solitary nucleus connectivity to key autonomic regions in humans. *Eur. J. Neurosci.* **56**, 3938–3966 (2022).
40. Jensen, D. E. A., Ebmeier, K. P., Suri, S., Rushworth, M. F. S. & Klein-Flugge, M. C. Nuclei-specific hypothalamus networks predict a dimensional marker of stress in humans. *Nat. Commun.* **15**, 2426 (2024).
41. Riverol, M. et al. Structural neuroimaging changes associated with subjective cognitive decline from a clinical sample. *Neuroimage Clin.* **42**, 103615 (2024).
42. Liu, W. et al. The whole-brain structural and functional connectome in Alzheimer's disease spectrum: a multimodal Bayesian meta-analysis of graph theoretical characteristics. *Neurosci. Biobehav. Rev.* **174**, 106174 (2025).
43. Mu, Y. & Gage, F. H. Adult hippocampal neurogenesis and its role in Alzheimer's disease. *Mol. Neurodegener.* **6**, 85 (2011).
44. Barkhof, F., Haller, S. & Rombouts, S. A. Resting-state functional MR imaging: a new window to the brain. *Radiology* **272**, 29–49 (2014).
45. Hu, G. et al. Trunk versus extremity adiposity and cardiometabolic risk factors in White and African American adults. *Diabetes Care* **34**, 1415–1418 (2011).
46. Qiu, Z. et al. Associations of regional body fat with risk of cardiovascular disease and mortality among individuals with Type 2 diabetes. *J. Clin. Endocrinol. Metab.* <https://doi.org/10.1210/clinem/dgae192> (2024).
47. Salat, D. H. et al. Thinning of the cerebral cortex in aging. *Cereb. Cortex* **14**, 721–730 (2004).
48. McGinnis, S. M., Brickhouse, M., Pascual, B. & Dickerson, B. C. Age-related changes in the thickness of cortical zones in humans. *Brain Topogr.* **24**, 279–291 (2011).
49. De Silva, S., Turner, B. J. & Perera, N. D. Metabolic dysfunction in motor neuron disease: shedding light through the lens of autophagy. *Metabolites* **12**, 574 (2022).

50. Hehl, M., Swinnen, S. P. & Cuypers, K. Alterations of hand sensorimotor function and cortical motor representations over the adult lifespan. *Aging (Albany NY)* **12**, 4617–4640 (2020).
51. Catani, M., Dell'acqua, F. & Thiebaut de Schotten, M. A revised limbic system model for memory, emotion and behaviour. *Neurosci. Biobehav. Rev.* **37**, 1724–1737 (2013).
52. Sanchez-Lopez, M. et al. Leg fat might be more protective than arm fat in relation to lipid profile. *Eur. J. Nutr.* **52**, 489–495 (2013).
53. Karpe, F. & Pinnick, K. E. Biology of upper-body and lower-body adipose tissue—link to whole-body phenotypes. *Nat. Rev. Endocrinol.* **11**, 90–100 (2015).
54. Caron, A., Lee, S., Elmquist, J. K. & Gautron, L. Leptin and brain-adipose crosstalks. *Nat. Rev. Neurosci.* **19**, 153–165 (2018).
55. Morrison, C. D. Leptin signaling in brain: a link between nutrition and cognition? *Biochim. Biophys. Acta* **1792**, 401–408 (2009).
56. Farr, O. M. et al. Leptin therapy alters appetite and neural responses to food stimuli in brain areas of leptin-sensitive subjects without altering brain structure. *J. Clin. Endocrinol. Metab.* **99**, E2529–E2538 (2014).
57. Scheja, L. & Heeren, J. The endocrine function of adipose tissues in health and cardiometabolic disease. *Nat. Rev. Endocrinol.* **15**, 507–524 (2019).
58. Khairova, R. A., Machado-Vieira, R., Du, J. & Manji, H. K. A potential role for pro-inflammatory cytokines in regulating synaptic plasticity in major depressive disorder. *Int. J. Neuropsychopharmacol.* **12**, 561–578 (2009).
59. Fjell, A. M. & Walhovd, K. B. Structural brain changes in aging: courses, causes and cognitive consequences. *Rev. Neurosci.* **21**, 187–221 (2010).
60. Lockhart, S. N. & DeCarli, C. Structural imaging measures of brain aging. *Neuropsychol. Rev.* **24**, 271–289 (2014).
61. Miller, E. K. & Cohen, J. D. An integrative theory of prefrontal cortex function. *Annu. Rev. Neurosci.* **24**, 167–202 (2001).
62. Friedman, N. P. & Robbins, T. W. The role of prefrontal cortex in cognitive control and executive function. *Neuropsychopharmacology* **47**, 72–89 (2022).
63. Yu, M. H., Lim, J. S., Yi, H. A., Won, K. S. & Kim, H. W. Association between visceral adipose tissue metabolism and cerebral glucose metabolism in patients with cognitive impairment. *Int. J. Mol. Sci.* **25**, 7479 (2024).
64. Cavedo, E. et al. Sex differences in functional and molecular neuroimaging biomarkers of Alzheimer's disease in cognitively normal older adults with subjective memory complaints. *Alzheimers Dement.* **14**, 1204–1215 (2018).
65. Rask-Andersen, M., Karlsson, T., Ek, W. E. & Johansson, A. Genome-wide association study of body fat distribution identifies adiposity loci and sex-specific genetic effects. *Nat. Commun.* **10**, 339 (2019).
66. Zhang, D. et al. Long-term obesity impacts brain morphology, functional connectivity and cognition in adults. *Nat. Mental Health* **3**, 466–478 (2025).
67. Borga, M. et al. Advanced body composition assessment: from body mass index to body composition profiling. *J. Investig. Med.* **66**, 1–9 (2018).
68. Dekkers, I. A., Jansen, P. R. & Lamb, H. J. Obesity, brain volume and white matter microstructure at MRI: a cross-sectional UK Biobank study. *Radiology* **291**, 763–771 (2019).
69. Miller, K. L. et al. Multimodal population brain imaging in the UK Biobank prospective epidemiological study. *Nat. Neurosci.* **19**, 1523–1536 (2016).
70. Reuter, M., Schmansky, N. J., Rosas, H. D. & Fischl, B. Within-subject template estimation for unbiased longitudinal image analysis. *NeuroImage* **61**, 1402–1418 (2012).
71. Finn, E. S. et al. Functional connectome fingerprinting: identifying individuals using patterns of brain connectivity. *Nat. Neurosci.* **18**, 1664–1671 (2015).
72. Achard, S. & Bullmore, E. Efficiency and cost of economical brain functional networks. *PLoS Comput. Biol.* **3**, e17 (2007).
73. He, Y., Chen, Z. & Evans, A. Structural insights into aberrant topological patterns of large-scale cortical networks in Alzheimer's disease. *J. Neurosci.* **28**, 4756–4766 (2008).
74. Wang, J. et al. Parcellation-dependent small-world brain functional networks: a resting-state fMRI study. *Hum. Brain Mapp.* **30**, 1511–1523 (2009).
75. Bielczyk, N. Z. et al. Thresholding functional connectomes by means of mixture modeling. *NeuroImage* **171**, 402–414 (2018).
76. Rubinov, M. & Sporns, O. Complex network measures of brain connectivity: uses and interpretations. *NeuroImage* **52**, 1059–1069 (2010).
77. Yeo, B. T. et al. The organization of the human cerebral cortex estimated by intrinsic functional connectivity. *J. Neurophysiol.* **106**, 1125–1165 (2011).
78. Daducci, A. et al. Accelerated microstructure imaging via convex optimization (AMICO) from diffusion MRI data. *NeuroImage* **105**, 32–44 (2015).
79. Fawcett-Ritchie, C. & Deary, I. J. Reliability and validity of the UK Biobank cognitive tests. *PLoS ONE* **15**, e0231627 (2020).
80. Shen, C., Liu, C. & Qiu, A. Metabolism-related brain morphology accelerates aging and predicts neurodegenerative diseases and stroke: a UK Biobank study. *Transl. Psychiatry* **13**, 233 (2023).
81. Han, Y. P. et al. Relationship between obesity and structural brain abnormality: accumulated evidence from observational studies. *Ageing Res. Rev.* **71**, 101445 (2021).
82. Raji, C. A. et al. Brain structure and obesity. *Hum. Brain Mapp.* **31**, 353–364 (2010).
83. Gomez-Apo, E., Mondragon-Maya, A., Ferrari-Diaz, M. & Silva-Pereyra, J. Structural brain changes associated with overweight and obesity. *J. Obes.* **2021**, 6613385 (2021).
84. Guan, S., Jiang, R., Meng, C. & Biswal, B. Brain age prediction across the human lifespan using multimodal MRI data. *GeroScience* **46**, 1–20 (2024).
85. Liang, H., Zhang, F. & Niu, X. Investigating systematic bias in brain age estimation with application to post-traumatic stress disorders. *Hum. Brain Mapp.* **40**, 3143–3152 (2019).
86. Le, T. T. et al. A nonlinear simulation framework supports adjusting for age when analyzing BrainAGE. *Front. Aging Neurosci.* **10**, 317 (2018).

Acknowledgements

This research is supported by the STI 2030 – Major Project (project no. 2022ZD0209000; A.Q.). Additional support is provided by the RGC GRF project (project no. 15201124; A.Q.) and the Hong Kong Global STEM Scholar scheme (A.Q.). This research was conducted using the UK Biobank resource under application no. 57831. We thank the UK Biobank participants and staff (UK Biobank Coordinating Centre, Stockport, UK).

Author contributions

A.Q. conceived and supervised the study. A.Q., D.Z., Y.F., C.S., C.L., N.C., H.C. and K.K.L. jointly developed the study concept and design. Data analyses were conducted by D.Z., Y.F., C.S. and C.L., with C.S. also responsible for data visualization. A.Q., D.Z. and Y.F. contributed to the interpretation of findings and the framing of the discussion. All authors contributed to drafting and revising the manuscript.

Competing interests

The authors declare no competing interests.

Additional information

Supplementary information The online version contains supplementary material available at
<https://doi.org/10.1038/s44220-025-00501-8>.

Correspondence and requests for materials should be addressed to Anqi Qiu.

Peer review information *Nature Mental Health* thanks Wyllians Vendramini Borelli, Robyn A. Honea and Géraldine Poisnel for their contribution to the peer review of this work.

Reprints and permissions information is available at www.nature.com/reprints.

Publisher's note Springer Nature remains neutral with regard to jurisdictional claims in published maps and institutional affiliations.

Open Access This article is licensed under a Creative Commons Attribution-NonCommercial-NoDerivatives 4.0 International License, which permits any non-commercial use, sharing, distribution and reproduction in any medium or format, as long as you give appropriate credit to the original author(s) and the source, provide a link to the Creative Commons licence, and indicate if you modified the licensed material. You do not have permission under this licence to share adapted material derived from this article or parts of it. The images or other third party material in this article are included in the article's Creative Commons licence, unless indicated otherwise in a credit line to the material. If material is not included in the article's Creative Commons licence and your intended use is not permitted by statutory regulation or exceeds the permitted use, you will need to obtain permission directly from the copyright holder. To view a copy of this licence, visit <http://creativecommons.org/licenses/by-nc-nd/4.0/>.

© The Author(s) 2025

Reporting Summary

Nature Portfolio wishes to improve the reproducibility of the work that we publish. This form provides structure for consistency and transparency in reporting. For further information on Nature Portfolio policies, see our [Editorial Policies](#) and the [Editorial Policy Checklist](#).

Statistics

For all statistical analyses, confirm that the following items are present in the figure legend, table legend, main text, or Methods section.

n/a Confirmed

- The exact sample size (n) for each experimental group/condition, given as a discrete number and unit of measurement
- A statement on whether measurements were taken from distinct samples or whether the same sample was measured repeatedly
- The statistical test(s) used AND whether they are one- or two-sided
Only common tests should be described solely by name; describe more complex techniques in the Methods section.
- A description of all covariates tested
- A description of any assumptions or corrections, such as tests of normality and adjustment for multiple comparisons
- A full description of the statistical parameters including central tendency (e.g. means) or other basic estimates (e.g. regression coefficient) AND variation (e.g. standard deviation) or associated estimates of uncertainty (e.g. confidence intervals)
- For null hypothesis testing, the test statistic (e.g. F , t , r) with confidence intervals, effect sizes, degrees of freedom and P value noted
Give P values as exact values whenever suitable.
- For Bayesian analysis, information on the choice of priors and Markov chain Monte Carlo settings
- For hierarchical and complex designs, identification of the appropriate level for tests and full reporting of outcomes
- Estimates of effect sizes (e.g. Cohen's d , Pearson's r), indicating how they were calculated

Our web collection on [statistics for biologists](#) contains articles on many of the points above.

Software and code

Policy information about [availability of computer code](#)

Data collection No software was used.

Data analysis MATLAB R2017b can be download at <https://www.mathworks.com>.
 FSL (version 5.0.10) can be download at <https://fsl.fmrib.ox.ac.uk/fsl/oldwiki/>.
 Freesurfer (version 7.1.1) can be download at <https://surfer.nmr.mgh.harvard.edu/>.
 Python 3.6 (<https://www.python.org/>) and R software (4.3.1; <https://cran.r-project.org/>) were used for statistical analysis (linear regression, Mann-Whitney U test and chi-squared test) and visualization.
 The R package 'lavaan' (version 0.6-19; <https://cran.r-project.org/web/packages/lavaan/index.html>) was used to perform the mediation analysis.
 The study employed linear regression and mediation analysis implemented in R (version 4.3.1). The code for these two models is available (https://github.com/fuyingji102/regional_adiposity).

For manuscripts utilizing custom algorithms or software that are central to the research but not yet described in published literature, software must be made available to editors and reviewers. We strongly encourage code deposition in a community repository (e.g. GitHub). See the Nature Portfolio [guidelines for submitting code & software](#) for further information.

Data

Policy information about [availability of data](#)

All manuscripts must include a [data availability statement](#). This statement should provide the following information, where applicable:

- Accession codes, unique identifiers, or web links for publicly available datasets
- A description of any restrictions on data availability
- For clinical datasets or third party data, please ensure that the statement adheres to our [policy](#)

The UK Biobank data is a public health database. This work mainly includes demographic data, obesity measures derived from dual-energy X-ray absorptiometry (DXA), brain images, and cognitive tests. Researchers can apply for access to the data on the UK Biobank website (<https://www.ukbiobank.ac.uk>). Additional information regarding registration for data access is available at <http://www.ukbiobank.ac.uk/register-apply/>. The application number for this study is 57831.

Research involving human participants, their data, or biological material

Policy information about studies with [human participants or human data](#). See also policy information about [sex, gender \(identity/presentation\), and sexual orientation](#) and [race, ethnicity and racism](#).

Reporting on sex and gender

This study use "sex" in the paper.

Reporting on race, ethnicity, or other socially relevant groupings

This study categorized ethnicity as white and non-white.

Population characteristics

This study leveraged publicly accessible demographic, phenotypic, image, and cognitive data from the UK Biobank, ensuring compliance with its ethical and data access guidelines. A detailed flowchart of participant selection is provided in Supplementary Fig. 1. During the first imaging visit, both DXA and brain MRI examinations were conducted. For this study, we identified 47,764 participants with available AFP, TFP, and LFP data and 40,072 participants with VAT measurements. We excluded participants who had major physical, neurological, or psychiatric disorders (Supplementary Methods), as well as those whose MRI scans did not meet quality standards. This resulted in analytic samples of 23,088 participants (mean age = 62.5 ± 7.40 years, standard deviation; 45.2% male participants) and 18,886 participants (mean age = 62.5 ± 7.43 years, standard deviation; 45.7% male participants) for fat percentage and VAT analyses, respectively. These analyses aimed to investigate the associations between regional adiposity measures and brain imagining metrics. Furthermore, participants who underwent cognitive function assessments at the assessment centers were selected to explore the relationships among regional adiposity, brain aging, and cognitive performance.

Recruitment

This study utilized data from the UK Biobank recruitment, encompassing over 500,000 participants aged 40 years in the United Kingdom at baseline. For more detailed information, please refer to <http://www.ukbiobank.ac.uk>.

Ethics oversight

We analysed data from the UK Biobank (application no. 57831), a nationwide population cohort that enrolled more than 500,000 adults at assessment centres across the United Kingdom between 2006 and 2010. The present analyses were conducted under the ethical approval granted to UK Biobank by the UK National Health Service National Research Ethics Service (reference 11/NW/0382). All participants provided written informed consent and could withdraw at any time without explanation. Study-related risk was considered minimal; however, UK Biobank maintains insurance arrangements that provide compensation for injuries arising from negligent conduct during participation.

Note that full information on the approval of the study protocol must also be provided in the manuscript.

Field-specific reporting

Please select the one below that is the best fit for your research. If you are not sure, read the appropriate sections before making your selection.

Life sciences

Behavioural & social sciences

Ecological, evolutionary & environmental sciences

For a reference copy of the document with all sections, see nature.com/documents/nr-reporting-summary-flat.pdf

Life sciences study design

All studies must disclose on these points even when the disclosure is negative.

Sample size

No formal sample size calculation was performed. All eligible participants were included from the publicly available UK Biobank dataset, comprising 23,088 participants with AFP, LFP, and TFP measurements and 18,886 participants with VAT measurements. The large sample size provides adequate statistical power, substantially exceeds that of similar studies, and ensures the robustness of the findings.

Data exclusions

To examine the relationships between these adiposity measures and brain imaging metrics in a non-clinical adult sample, we further selected participants with multi-modal brain magnetic resonance imaging (MRI) data and excluded those with major physical, neurological, or psychiatric diseases (Supplementary Fig. 1).

Replication

All available data were used to maximize statistical power of the analysis therefore we did not repeat the analysis.

Randomization

In this study, covariates were selected based on their potential associations with obesity and brain characteristics, as reported in previous research. Age at the time of the imaging visit (the second follow-up wave) was included as a covariate. Additional baseline covariates encompassed demographics (sex, ethnicity, and handedness), socioeconomic status (years of education and employment status), lifestyle factors (physical activity, smoking frequency, and alcohol consumption frequency), and metabolic health, represented by the metabolic syndrome score. At the imaging visit, MRI scanning centers were considered to account for variability in imaging equipment, brain size was included to adjust for differences in brain morphology, and mean framewise displacement was included to control for head motion. Imaging sites (Cheadle, Reading, and Newcastle) were also included as a covariate to control potential differences due to scanner variability. More details can be found in the Supplementary Methods.

Blinding

Blinding was not applicable to this study as this study is observational.

Reporting for specific materials, systems and methods

We require information from authors about some types of materials, experimental systems and methods used in many studies. Here, indicate whether each material, system or method listed is relevant to your study. If you are not sure if a list item applies to your research, read the appropriate section before selecting a response.

Materials & experimental systems

- | | |
|-------------------------------------|--|
| n/a | Involved in the study |
| <input checked="" type="checkbox"/> | <input type="checkbox"/> Antibodies |
| <input checked="" type="checkbox"/> | <input type="checkbox"/> Eukaryotic cell lines |
| <input checked="" type="checkbox"/> | <input type="checkbox"/> Palaeontology and archaeology |
| <input checked="" type="checkbox"/> | <input type="checkbox"/> Animals and other organisms |
| <input checked="" type="checkbox"/> | <input type="checkbox"/> Clinical data |
| <input checked="" type="checkbox"/> | <input type="checkbox"/> Dual use research of concern |
| <input checked="" type="checkbox"/> | <input type="checkbox"/> Plants |

Methods

- | | |
|-------------------------------------|--|
| n/a | Involved in the study |
| <input checked="" type="checkbox"/> | <input type="checkbox"/> ChIP-seq |
| <input checked="" type="checkbox"/> | <input type="checkbox"/> Flow cytometry |
| <input type="checkbox"/> | <input checked="" type="checkbox"/> MRI-based neuroimaging |

Plants

Seed stocks

N/A

Novel plant genotypes

N/A

Authentication

N/A

Magnetic resonance imaging

Experimental design

Design type

Structural MRI, resting-state functional MRI, neurite orientation dispersion and density imaging (NODDI)

Design specifications

UK Biobank designed the imaging acquisition protocols including 6 modalities. This study primarily utilized T1-weighted structural images, resting-state functional MRI and diffusion-weighted imaging (DWI) images from these protocols.

Behavioral performance measures

N/A

Acquisition

Imaging type(s)	Structural MRI, resting-state functional MRI, diffusion-weighted imaging (DWI)
Field strength	3T
Sequence & imaging parameters	The T1-weighted image was obtained using Magnetization Prepared Rapid Acquisition Gradient-Echo (MPRAGE) with 1×1mm resolution, a field-of-view of 208 × 256 × 256 mm, TI/TR/TE of 880/2000/2.01 ms, and a flip angle of 8°. Resting-state fMRI (rs-fMRI) was acquired using gradient echo EPI (GE-EPI), interleaved multi-slice, gradient-echo, echo planar imaging (GE-EPI) sequence with 8 multislice acceleration; TR = 0.735 s, TE = 39 ms, flip angle = 52°, matrix = 88 × 88, resolution = 2.4 mm × 2.4 mm; slice thickness = 2.4 mm; slice number = 64 slices; rs-fMRI acquisition time = 6 minutes. The standardized parameters can be referenced at https://biobank.ctsu.ox.ac.uk/crystal/crystal/docs/brain_mri.pdf .
Area of acquisition	<i>State whether a whole brain scan was used OR define the area of acquisition, describing how the region was determined.</i>
Diffusion MRI	<input checked="" type="checkbox"/> Used <input type="checkbox"/> Not used

Preprocessing

Preprocessing software	Freesurfer (version 7.1.1) and FSL (version 5.0.10)
Normalization	large deformation diffeomorphic metric mapping (LDDMM)
Normalization template	fsaverage and the JHU MNI atlas
Noise and artifact removal	Before preprocessing, noisy images were removed from the study
Volume censoring	Before preprocessing, fMRI volumes with large motion were removed

Statistical modeling & inference

Model type and settings	linear regression model
Effect(s) tested	The standardized beta coefficients were obtained for the linear regression models.
Specify type of analysis:	<input checked="" type="checkbox"/> Whole brain <input type="checkbox"/> ROI-based <input type="checkbox"/> Both
Statistic type for inference	vertex-wise statistics, connectome statistics and volume-wise statistics
(See Eklund et al. 2016)	
Correction	FDR, random field theory [RFT] correction

Models & analysis

n/a	Involved in the study
<input type="checkbox"/>	<input checked="" type="checkbox"/> Functional and/or effective connectivity
<input checked="" type="checkbox"/>	<input type="checkbox"/> Graph analysis
<input checked="" type="checkbox"/>	<input type="checkbox"/> Multivariate modeling or predictive analysis
Functional and/or effective connectivity	Functional connectivity is measured using Pearson correlation